



**HAL**  
open science

## Linear complex polarization propagator in a four-component Kohn-Sham framework.

Sebastien Villaume, Trond Saue, Patrick Norman

► **To cite this version:**

Sebastien Villaume, Trond Saue, Patrick Norman. Linear complex polarization propagator in a four-component Kohn-Sham framework.. *Journal of Chemical Physics*, 2010, 133 (6), pp.064105. 10.1063/1.3461163 . hal-00760979

**HAL Id: hal-00760979**

**<https://hal.science/hal-00760979>**

Submitted on 21 Jan 2020

**HAL** is a multi-disciplinary open access archive for the deposit and dissemination of scientific research documents, whether they are published or not. The documents may come from teaching and research institutions in France or abroad, or from public or private research centers.

L'archive ouverte pluridisciplinaire **HAL**, est destinée au dépôt et à la diffusion de documents scientifiques de niveau recherche, publiés ou non, émanant des établissements d'enseignement et de recherche français ou étrangers, des laboratoires publics ou privés.

## Linear complex polarization propagator in a four-component Kohn–Sham framework

Sebastien Villaume, Trond Saue, and Patrick Norman

Citation: *The Journal of Chemical Physics* **133**, 064105 (2010); doi: 10.1063/1.3461163

View online: <http://dx.doi.org/10.1063/1.3461163>

View Table of Contents: <http://scitation.aip.org/content/aip/journal/jcp/133/6?ver=pdfcov>

Published by the [AIP Publishing](#)

---

### Articles you may be interested in

[A simple scheme for magnetic balance in four-component relativistic Kohn–Sham calculations of nuclear magnetic resonance shielding constants in a Gaussian basis](#)

*J. Chem. Phys.* **136**, 014108 (2012); 10.1063/1.3671390

[Role of noncollinear magnetization for the first-order electric-dipole hyperpolarizability at the four-component Kohn–Sham density functional theory level](#)

*J. Chem. Phys.* **130**, 024109 (2009); 10.1063/1.3054302

[Quadratic response functions in the relativistic four-component Kohn–Sham approximation](#)

*J. Chem. Phys.* **128**, 024105 (2008); 10.1063/1.2816709

[Polarization consistent basis sets. II. Estimating the Kohn–Sham basis set limit](#)

*J. Chem. Phys.* **116**, 7372 (2002); 10.1063/1.1465405

[The asymptotic exchange potential in Kohn–Sham theory](#)

*J. Chem. Phys.* **112**, 3507 (2000); 10.1063/1.480505

---



**AIP** | APL Photonics

*APL Photonics* is pleased to announce  
**Benjamin Eggleton** as its Editor-in-Chief



# Linear complex polarization propagator in a four-component Kohn–Sham framework

Sebastien Villaume,<sup>1</sup> Trond Saue,<sup>2</sup> and Patrick Norman<sup>1,a)</sup>

<sup>1</sup>*Department of Physics, Chemistry and Biology, Linköping University, SE-581 83 Linköping, Sweden*

<sup>2</sup>*Institut de Chimie de Strasbourg, Laboratoire de Chimie Quantique, CNRS et Université de Strasbourg, 4 rue Blaise Pascal, F-67070 Strasbourg, France*

(Received 4 May 2010; accepted 17 June 2010; published online 12 August 2010)

An algorithm for the solution of the linear response equation in the random phase approximation is presented. All entities including frequency arguments, matrices, and vectors, are assumed to be complex, and it represents the core equation solver needed in complex polarization propagator approaches where nonstimulated relaxation channels are taken into account. Stability and robustness of the algorithm are demonstrated in applications regarding visible, ultraviolet, and x-ray spectroscopies. An implementation of the algorithm at the level of four-component relativistic, noncollinear, density functional theory for imaginary (but not complex) frequency arguments has been achieved and is used to determine the electric dipole dispersion interaction coefficients for the rubidium and cesium dimers. Our best estimates for the  $C_6$  coefficients of  $\text{Rb}_2$  and  $\text{Cs}_2$  are equal to  $14.0 \times 10^3$  and  $21.9 \times 10^3$  a.u., respectively. © 2010 American Institute of Physics.

[doi:10.1063/1.3461163]

## I. INTRODUCTION

With the introduction of damping terms in the equations-of-motion, it is possible to take into account other molecular decay processes than stimulated emission in wave function theory.<sup>1</sup> In the presence of external electromagnetic fields of modest intensity, the excited state populations may, under such conditions, remain small even under resonance conditions, and the equations-of-motion can be solved by means of perturbation theory, giving rise to linear and nonlinear response functions (or polarization propagators) that determine the time-dependence of the polarization. The main characteristic of response functions associated with resonant external fields (as compared to the nonresonant situation) is the fact that they become complex-valued (instead of real-valued) with real and imaginary parts that are related by the Kramers–Kronig relation and associated with different spectroscopies. As a fundamental property of these response functions, one notes the fact that a sign inversion of optical frequencies is associated with the operation of complex conjugation.

From a mathematical and implementational point of view, the essential difference between the conventional nonresonant and the resonant cases amounts to a substitution of the real optical frequencies  $\omega$  for general complex arguments  $z$ . Considering the linear response function as an example, the needed generalization becomes

$$\langle\langle \hat{\Omega}; \hat{V}^\omega \rangle\rangle_\omega \Rightarrow \langle\langle \hat{\Omega}; \hat{V}^z \rangle\rangle_z, \quad (1)$$

where  $\hat{\Omega}$  and  $\hat{V}^\omega$  correspond to the observable of interest and the operator responsible for the coupling between the quantum mechanical system and the classical external field (os-

cillating with an angular frequency  $\omega$ ), respectively. Since the first formulation (based on the Ehrenfest theorem) and implementation of the complex linear response function was presented in the multiconfigurational self-consistent field approximation,<sup>1,2</sup> other implementations<sup>3–5</sup> including a quasienergy based formulation<sup>5</sup> have followed.

Numerous applications of the methodology have been published and the proven diversity is connected with various choices of operators and argument in Eq. (1) ( $z$  is here considered as the argument of the response function) in addition to the aforementioned fact that the real and imaginary parts of the complex response functions often are associated with separate spectroscopies. In optical electronic resonance spectroscopies, the argument is chosen as  $z = \omega + i\gamma$  which introduces a relaxation parameter  $\gamma$  that is connected with the inverse of the finite lifetimes of excited states. The observable is under normal circumstances equal to the polarization or magnetization ( $\hat{\Omega}$  equals the electric or magnetic dipole operator) and the coupling to the external fields is given in terms of multipole expansions ( $\hat{V}^\omega$  equals an electric or magnetic dipole, quadrupole, etc. operator). A selection of applications includes Raman scattering,<sup>6,7</sup> X-ray absorption<sup>8,9</sup> and natural circular dichroism,<sup>10,11</sup> optical rotatory dispersion,<sup>12</sup> and electronic circular dichroism.<sup>13–15</sup> If one, on the other hand, with the argument  $z$  associates an imaginary frequency  $i\omega$ , it becomes possible to address dispersion interactions from a perturbational treatment of electron interactions between two separated systems. With  $\hat{\Omega}$  as well as  $\hat{V}^\omega$  equal to the electric dipole operator, the response function becomes, in this case, associated with the  $C_6$  dipole-dipole dispersion coefficients.<sup>16</sup>

Clearly, from a general point of view, the extension of propagator theories in chemistry to consider relaxation mechanisms other than stimulated emission is quite indepen-

<sup>a)</sup>Electronic mail: panor@ifm.liu.se.

dent on the choice of electronic structure method—the work mentioned above includes calculations based on single (Hartree–Fock and Kohn–Sham) as well as multideterminant reference states—and on the system Hamiltonian. The latter aspect means that concerns of resonance fields are the same in the nonrelativistic and relativistic frameworks, although the implementations in the respective cases will of course differ in details, and it has been utilized by Devarajan *et al.*<sup>4</sup> for the implementation of the complex linear response function in the zeroth-order regular approximation. In the present work we will continue this line of development with the derivation and implementation of the linear complex polarization propagator (CPP) in the four-component relativistic noncollinear Kohn–Sham density functional theory (DFT) approximation. The development of a resonance-convergent propagator is of particular importance in the relativistic realm, since, due to the fact that spin is not conserved as a “good” quantum number, the density of excited states is much higher than in the nonrelativistic case (singlet and triplet manifolds of states cannot be treated separately). The consequence of a high density of states is that conventional response calculations are applicable only in narrow regions of the optical spectrum, since each transition energy is associated with a pole of the response function.

At the four-component level of theory, all entities, apart from the metric, in the random phase approximation (RPA) equation will be complex, and we will pay particular attention to the design of a linear equation solver that is stable and efficient for this general case. It is to be expected that this work will be valuable also in the nonrelativistic realm in concern with cubic (and higher-order) response functions, where the right-hand sides of the second-order response equations will be complex.

Example calculations will be provided in terms of the polarizability tensors of lithium hydride and the rubidium and cesium dimers. The former small system will be used to illustrate convergence in the linear response solver for a general complex argument  $z$  and for the latter two systems we will determine the  $C_6$ -coefficients.

## II. THEORY OF COMPLEX LINEAR RESPONSE EQUATION SOLVER

### A. General considerations

From a general perspective the formulation of a complex linear response solver can be done in an analogous manner to the case of real frequencies<sup>17,18</sup> by a mere substitution for a complex frequency argument, so let us briefly present the key equations involved in such a generalization. The linear response equation, or the random phase approximation (RPA) equation, reads as

$$(\mathbf{E}^{[2]} - z\mathbf{S}^{[2]})\mathbf{X}(z) = -\mathbf{E}_B^{[1]}, \quad (2)$$

where  $\mathbf{E}^{[2]}$ ,  $\mathbf{S}^{[2]}$ , and  $\mathbf{E}_B^{[1]}$  are known as the generalized Hessian, metric, and property gradient, respectively, and

$\mathbf{X}(z)$  is the solution vector also known as the linear response vector. In principle, the solution vector can be obtained by explicit matrix inversion but, in practice, due to the large dimension of the involved matrices, one is forced to adopt an iterative algorithm where the solution vector is expanded in a set of  $n$  trial vectors  $\{\mathbf{b}_k\}_{k=1}^n$  according to

$$\mathbf{X}_n(z) = \sum_{k=1}^n a_k(z)\mathbf{b}_k. \quad (3)$$

The optimal expansion coefficients are found by solving the  $n$ -dimensional reduced equation

$$(\tilde{\mathbf{E}}^{[2]} - z\tilde{\mathbf{S}}^{[2]})\mathbf{a} = -\tilde{\mathbf{E}}_B^{[1]}, \quad (4)$$

where  $\mathbf{a}$  is a vector collecting the amplitudes  $a_k(z)$  and the elements of the reduced Hessian and overlap matrices and the reduced gradient are given by  $\tilde{\mathbf{E}}_{ij}^{[2]} = \mathbf{b}_i^\dagger \mathbf{E}^{[2]} \mathbf{b}_j$ ,  $\tilde{\mathbf{S}}_{ij}^{[2]} = \mathbf{b}_i^\dagger \mathbf{S}^{[2]} \mathbf{b}_j$ , and  $\tilde{\mathbf{E}}_{B;i}^{[1]} = \mathbf{b}_i^\dagger \mathbf{E}_B^{[1]}$ , respectively. In a given iteration  $n$ , one defines a residual  $\mathbf{R}_n(z)$  from the approximate solution vector  $\mathbf{X}_n(z)$  according to

$$\mathbf{R}_n(z) = (\mathbf{E}^{[2]} - z\mathbf{S}^{[2]})\mathbf{X}_n(z) + \mathbf{E}_B^{[1]}, \quad (5)$$

where we note that, in the initial iteration the residual will become equal to  $\mathbf{R}_0 = \mathbf{E}_B^{[1]}$ . Given that the norm of the residual exceeds a threshold value (if not, the iterations are terminated), the residual in Eq. (5) is used to generate an additional trial vector for the next iteration. This generation is based on the assumption that the Hessian and the metric are diagonal dominant (and that we have access to these diagonal elements)

$$\mathbf{b}_{n+1} = -[\text{diag}(\mathbf{E}^{[2]} - z\mathbf{S}^{[2]})]^{-1}\mathbf{R}_n. \quad (6)$$

In the RPA, the metric is indeed diagonal (reflecting orthogonality between Slater determinants), whereas the Hessian is only diagonal dominant (reflecting that the Slater determinants are not eigenstates of the Hamiltonian). The singularities of the RPA matrix in Eq. (2) are found for  $z = \pm \hbar\omega_{n0}$  ( $n=1, 2, \dots$ ) corresponding to the plus and minus the excitation energies of the system, and, it is clear that, for large  $z$  far from singular points, the approximation of a diagonal RPA matrix is an excellent one and the added trial vector should bring us close to the true solution and convergence in the iterative scheme.

### B. Four-component relativistic framework

The linear response equations outlined above are based on a unitary exponential parametrization of the Hartree–Fock or Kohn–Sham determinant such that a perturbed occupied orbital is given by

$$\tilde{\phi}_i(\kappa) = \sum_a \phi_a[\exp(-\kappa)]_{ai}, \quad (7)$$

where indices  $i$  and  $a$  refer to occupied and virtual orbitals, respectively. Such a parametrization has the advantage of allowing unconstrained optimization techniques and the straightforward identification of redundancies, in particular the occupied-occupied and virtual-virtual blocks of the anti-Hermitian orbital rotation matrix  $\kappa$  may be set to zero. In the relativistic realm the orbital rotation parameters naturally split into two classes  $\kappa_{ai}^{++}$  and  $\kappa_{ai}^{--}$  according to whether the virtual orbital is of positive or negative energy, respectively.

In the implementation of the linear response equation solver, there are certain symmetries to be exploited. The origin of these symmetries lies in the quantum mechanical operators and wave functions and they are manifested in matrix and vector structures. In the closed-shell four-component single determinant approximation, time-reversal symmetry of the zeroth-order wave function is ensured by occupation of Kramers pair orbitals related by

$$\phi_{\bar{p}}(\mathbf{r}) = \hat{\mathcal{K}}\phi_p(\mathbf{r}), \quad \hat{\mathcal{K}} = -i\Sigma_y\hat{\mathcal{K}}_0, \quad \Sigma_y = \begin{bmatrix} \sigma_y & 0_2 \\ 0_2 & \sigma_y \end{bmatrix}, \quad (8)$$

where  $\hat{\mathcal{K}}_0$  denote the complex conjugation operator and  $\Sigma_y$  is the four-component equivalent of the Pauli spin matrix  $\sigma_y$ . In the nonrelativistic realm using real orbitals this corresponds to the  $\alpha$ - and  $\beta$ -spin orbitals.

Within this framework, let us first consider a property gradient that takes the form

$$\mathbf{E}_B^{[1]} = \begin{bmatrix} \mathbf{g}^B \\ \mathbf{g}^{B*} \end{bmatrix}, \quad g_{ai}^B = -h_{B;ai}. \quad (9)$$

The elements of the property gradient vector are selected from the matrix representation  $h_B$  of the corresponding property operator. Since the operators have well-defined Hermiticity  $h$  and time-reversal symmetry  $t$ , these symmetries are conferred to the property gradient and will lead to a vector structure of the form<sup>18,19</sup>

$$\mathbf{G}^{(h,t)} = [\mathbf{c} \ \mathbf{d} \ \mathbf{tc}^* \ -\mathbf{td}^* \ \mathbf{hc}^* \ \mathbf{hd}^* \ \mathbf{htc} \ -\mathbf{htd}]^T. \quad (10)$$

Segment  $\mathbf{c}$  arises from electronic excitations between unbarred orbitals; segment  $\mathbf{d}$  arises from excitations from unbarred to barred orbitals; segment  $\mathbf{tc}^*$  arises from excitations between barred orbitals; and segment  $-\mathbf{td}^*$  arises from excitations from barred to unbarred orbitals. The four remaining segments refer to the corresponding de-excitations.

With the corresponding ordering of excitation and de-excitation operators, the matrix structures of the Hessian and overlap matrices will read as

$$\mathbf{E}^{[2]} = \begin{bmatrix} A_{11} & A_{12} & A_{13} & A_{14} & B_{11} & B_{12} & B_{13} & B_{14} \\ A_{12}^\dagger & A_{22} & -A_{14}^T & A_{24} & B_{12}^T & B_{22} & -B_{14}^\dagger & B_{24} \\ A_{13}^* & -A_{14}^* & A_{11}^* & -A_{12}^* & B_{13}^* & -B_{14}^* & B_{11}^* & -B_{12}^* \\ A_{14}^\dagger & A_{24} & -A_{12}^T & A_{22} & B_{14}^T & B_{24} & -B_{12}^\dagger & B_{22}^* \\ B_{11}^* & B_{12}^* & B_{13}^* & B_{14}^* & A_{11}^* & A_{12}^* & A_{13}^* & A_{14}^* \\ B_{12}^\dagger & B_{22}^* & -B_{14}^T & B_{24}^* & A_{12}^T & A_{22}^* & -A_{14}^\dagger & A_{24}^* \\ B_{13} & -B_{14} & B_{11} & -B_{12} & A_{13} & -A_{14} & A_{11} & -A_{12} \\ B_{14}^\dagger & B_{24} & -B_{12}^T & B_{22} & A_{14}^T & A_{24} & -A_{12}^\dagger & A_{22} \end{bmatrix} \quad (11)$$

and

$$\mathbf{S}^{[2]} = \begin{bmatrix} \Sigma_{11} & \Sigma_{12} & \Sigma_{13} & \Sigma_{14} & \Delta_{11} & \Delta_{12} & \Delta_{13} & \Delta_{14} \\ \Sigma_{12}^\dagger & \Sigma_{22} & -\Sigma_{14}^T & \Sigma_{24} & -\Delta_{12}^T & \Delta_{22} & \Delta_{14}^\dagger & \Delta_{24} \\ \Sigma_{13}^* & -\Sigma_{14}^* & \Sigma_{11}^* & -\Sigma_{12}^* & \Delta_{13}^* & -\Delta_{14}^* & \Delta_{11}^* & -\Delta_{12}^* \\ \Sigma_{14}^\dagger & \Sigma_{24} & -\Sigma_{12}^T & \Sigma_{22} & -\Delta_{14}^T & \Delta_{24}^* & \Delta_{12}^\dagger & \Delta_{22}^* \\ -\Delta_{11}^* & -\Delta_{12}^* & -\Delta_{13}^* & -\Delta_{14}^* & -\Sigma_{11}^* & -\Sigma_{12}^* & -\Sigma_{13}^* & -\Sigma_{14}^* \\ \Delta_{12}^\dagger & -\Delta_{22}^* & -\Delta_{14}^T & -\Delta_{24}^* & -\Sigma_{12}^T & -\Sigma_{22}^* & \Sigma_{14}^\dagger & -\Sigma_{24}^* \\ -\Delta_{13} & \Delta_{14} & -\Delta_{11} & \Delta_{12} & -\Sigma_{13} & \Sigma_{14} & -\Sigma_{11} & \Sigma_{12} \\ \Delta_{14}^\dagger & -\Delta_{24} & -\Delta_{12}^T & -\Delta_{22} & -\Sigma_{14}^T & -\Sigma_{24} & \Sigma_{12}^\dagger & -\Sigma_{22}^* \end{bmatrix}, \quad (12)$$

respectively, and it becomes straightforward to show that, when multiplying a vector  $\mathbf{U}^{(h,t)}$ , both  $\mathbf{E}^{[2]}$  and  $\mathbf{S}^{[2]}$  conserve time-reversal symmetry, but  $\mathbf{S}^{[2]}$  will reverse the hermicity<sup>18,19</sup>

$$\begin{aligned}\mathbf{E}^{[2]}\mathbf{U}^{(h,t)} &= \mathbf{U}^{(h,t)}, \\ \mathbf{S}^{[2]}\mathbf{U}^{(h,t)} &= \mathbf{U}^{(-h,t)}.\end{aligned}\quad (13)$$

As will be shown shortly, for a nonzero complex frequency  $z$ , the solution vector will have neither a well-defined Hermiticity nor a well-defined time-reversal symmetry. However, the solution vector can always be uniquely decomposed into four symmetry-adapted components according to

$$\mathbf{X} = \mathbf{X}^{++} + \mathbf{X}^{-+} + \mathbf{X}^{+-} + \mathbf{X}^{--}, \quad (14)$$

where, here and elsewhere, the first and second signs correspond to Hermiticity and time-reversal symmetry, respectively.

Let us illustrate the effects of the decomposition in Eq. (14) in the case of a perturbation that is associated with a Hermitian  $h=+1$  and time-reversal symmetric  $t=+1$  operator (e.g., the coupling to an external electric field). The corresponding property gradient will be designated by  $\mathbf{E}_B^{[1]++}$ , and due to Eqs. (10), (13), and (14), we can rewrite the linear response equation [Eq. (2)] as a system of four coupled equations

$$\begin{aligned}\mathbf{E}^{[2]}\mathbf{X}^{++} - \omega\mathbf{S}^{[2]}\mathbf{X}^{-+} - i\gamma\mathbf{S}^{[2]}\mathbf{X}^{+-} &= -\mathbf{E}_B^{[1]++}, \\ \mathbf{E}^{[2]}\mathbf{X}^{-+} - \omega\mathbf{S}^{[2]}\mathbf{X}^{++} - i\gamma\mathbf{S}^{[2]}\mathbf{X}^{--} &= \mathbf{0}, \\ \mathbf{E}^{[2]}\mathbf{X}^{+-} - \omega\mathbf{S}^{[2]}\mathbf{X}^{--} - i\gamma\mathbf{S}^{[2]}\mathbf{X}^{++} &= \mathbf{0}, \\ \mathbf{E}^{[2]}\mathbf{X}^{--} - \omega\mathbf{S}^{[2]}\mathbf{X}^{+-} - i\gamma\mathbf{S}^{[2]}\mathbf{X}^{-+} &= \mathbf{0}.\end{aligned}\quad (15)$$

Inspection of these equations shows that, the general case of a complex frequency  $z$  will involve all four symmetry-adapted components of the solution vector. In the case of a real frequency  $\omega$ , on the other hand, only components  $\mathbf{X}^{++}$  and  $\mathbf{X}^{-+}$  need to be considered, and, the case of an imaginary frequency  $i\gamma$  involves  $\mathbf{X}^{++}$  and  $\mathbf{X}^{+-}$ . The imposition of structure (due to Hermiticity and time-reversal symmetry) on the corresponding trial vectors has been detailed in Ref. 20 for the case of real frequencies, and the associated computational savings are discussed in this work.

Property operators are Hermitian  $h=+1$ , but may be time-reversal symmetric  $t=+1$  or time-reversal antisymmetric  $t=-1$ , typically corresponding to the coupling to electric and magnetic fields, respectively. However, in order to accommodate the quaternion packing scheme that has been developed for the handling of symmetries in the four-component realm,<sup>21</sup> we convert time-reversal antisymmetric elements into symmetric ones by extracting an imaginary phase according to

$$\mathbf{U}^{h,t} = i\bar{\mathbf{U}}^{-h,-t} \quad (16)$$

thus reversing the sign of both  $h$  and  $t$ . We will keep track of this change by using a bar notation as exemplified above. At the end of the calculation, the imaginary phase is to be reinserted to retain the original set of elements. When applied to the solution vector, we get

$$\mathbf{X} = \mathbf{X}^{++} + \mathbf{X}^{-+} + i(\bar{\mathbf{X}}^{-+} + \bar{\mathbf{X}}^{++}) \quad (17)$$

and the set of coupled equations will become equal to

$$\begin{aligned}\mathbf{E}^{[2]}\mathbf{X}^{++} - \omega\mathbf{S}^{[2]}\mathbf{X}^{-+} + \gamma\mathbf{S}^{[2]}\bar{\mathbf{X}}^{-+} &= -\mathbf{E}_B^{[1]++}, \\ \mathbf{E}^{[2]}\mathbf{X}^{-+} - \omega\mathbf{S}^{[2]}\mathbf{X}^{++} + \gamma\mathbf{S}^{[2]}\bar{\mathbf{X}}^{++} &= \mathbf{0}, \\ \mathbf{E}^{[2]}\bar{\mathbf{X}}^{-+} - \omega\mathbf{S}^{[2]}\bar{\mathbf{X}}^{++} - \gamma\mathbf{S}^{[2]}\mathbf{X}^{++} &= \mathbf{0}, \\ \mathbf{E}^{[2]}\bar{\mathbf{X}}^{++} - \omega\mathbf{S}^{[2]}\bar{\mathbf{X}}^{-+} - \gamma\mathbf{S}^{[2]}\mathbf{X}^{-+} &= \mathbf{0}.\end{aligned}\quad (18)$$

We note that, from this point onwards, all quantities are time-reversal symmetric and we may drop the superscript referring to time-reversal symmetry. The four components of the solution vector, i.e.,  $\mathbf{X}^+$ ,  $\mathbf{X}^-$ ,  $\bar{\mathbf{X}}^+$ , and  $\bar{\mathbf{X}}^-$ , are expanded in two sets of orthonormal trial vectors of different Hermiticity ( $\{\mathbf{b}_k^+\}_{k=1}^p$  and  $\{\mathbf{b}_k^-\}_{k=1}^m$ )

$$\begin{aligned}\mathbf{X}^+ &= \sum_{k=1}^p a_k^+ \mathbf{b}_k^+, & \bar{\mathbf{X}}^+ &= \sum_{k=1}^p \bar{a}_k^+ \mathbf{b}_k^+, \\ \mathbf{X}^- &= \sum_{k=1}^m a_k^- \mathbf{b}_k^-, & \bar{\mathbf{X}}^- &= \sum_{k=1}^m \bar{a}_k^- \mathbf{b}_k^-\end{aligned}\quad (19)$$

The coupled reduced equations thereby take the form

$$\begin{aligned}\begin{bmatrix} \tilde{\mathbf{E}}^{++} & -\omega\tilde{\mathbf{S}}^{+-} & \gamma\tilde{\mathbf{S}}^{+-} & \mathbf{0} \\ -\omega\tilde{\mathbf{S}}^{-+} & \tilde{\mathbf{E}}^{--} & \mathbf{0} & \gamma\tilde{\mathbf{S}}^{-+} \\ -\gamma\tilde{\mathbf{S}}^{-+} & \mathbf{0} & \tilde{\mathbf{E}}^{--} & -\omega\tilde{\mathbf{S}}^{-+} \\ \mathbf{0} & -\gamma\tilde{\mathbf{S}}^{+-} & -\omega\tilde{\mathbf{S}}^{+-} & \tilde{\mathbf{E}}^{++} \end{bmatrix} \begin{bmatrix} \mathbf{a}^+ \\ \mathbf{a}^- \\ \bar{\mathbf{a}}^- \\ \bar{\mathbf{a}}^+ \end{bmatrix} \\ = \begin{bmatrix} -\tilde{\mathbf{E}}_B^{[1]++} \\ \mathbf{0} \\ \mathbf{0} \\ \mathbf{0} \end{bmatrix},\end{aligned}\quad (20)$$

where  $\tilde{\mathbf{E}}^{++}$  and  $\tilde{\mathbf{E}}^{--}$  are square submatrices of dimensions  $p$  and  $m$ , respectively, and  $\tilde{\mathbf{S}}^{+-}$  and  $\tilde{\mathbf{S}}^{-+}$  are rectangular submatrices of dimensions  $(p \times m)$  and  $(m \times p)$ , respectively. It should be noted that the signs in the superscripts of the reduced matrices both correspond to Hermiticity, and that the reduced equation is purely real.

The residual defined in accordance with Eq. (5) is naturally decomposed into four components

$$\begin{aligned}
\mathbf{R}_n^+ &= \mathbf{E}^{[2]}\mathbf{X}_n^+ + \omega\mathbf{S}^{[2]}\mathbf{X}_n^- + \gamma\mathbf{S}^{[2]}\bar{\mathbf{X}}_n^- + \mathbf{E}_B^{[1]+}, \\
\mathbf{R}_n^- &= \mathbf{E}^{[2]}\mathbf{X}_n^- - \omega\mathbf{S}^{[2]}\mathbf{X}_n^+ + \gamma\mathbf{S}^{[2]}\bar{\mathbf{X}}_n^+, \\
\bar{\mathbf{R}}_n^- &= \mathbf{E}^{[2]}\bar{\mathbf{X}}_n^- - \omega\mathbf{S}^{[2]}\bar{\mathbf{X}}_n^+ - \gamma\mathbf{S}^{[2]}\mathbf{X}_n^+, \\
\bar{\mathbf{R}}_n^+ &= \mathbf{E}^{[2]}\bar{\mathbf{X}}_n^+ - \omega\mathbf{S}^{[2]}\bar{\mathbf{X}}_n^- - \gamma\mathbf{S}^{[2]}\mathbf{X}_n^-.
\end{aligned} \tag{21}$$

Following Eq. (6), we obtain additional trial vectors by the multiplication of the residual vector by a preconditioner in terms of the inverse of the diagonal of the RPA matrix. The assumption of a diagonal RPA matrix decomposes the above equations into a generally four-dimensional system of equations.

$$\begin{bmatrix} A_{ai,ai} & -\omega\Sigma_{ai,ai} & \gamma\Sigma_{ai,ai} & 0 \\ -\omega\Sigma_{ai,ai} & A_{ai,ai} & 0 & \gamma\Sigma_{ai,ai} \\ -\gamma\Sigma_{ai,ai} & 0 & A_{ai,ai} & -\omega\Sigma_{ai,ai} \\ 0 & -\gamma\Sigma_{ai,ai} & -\omega\Sigma_{ai,ai} & A_{ai,ai} \end{bmatrix} \begin{bmatrix} b_{p+1;ai}^+ \\ b_{m+1;ai}^- \\ b_{m+2;ai}^- \\ b_{p+2;ai}^+ \end{bmatrix} = \begin{bmatrix} -R_{n;ai}^+ \\ -R_{n;ai}^- \\ -\bar{R}_{n;ai}^- \\ -\bar{R}_{n;ai}^+ \end{bmatrix}. \tag{22}$$

Direct inversion gives the preconditioner

$$\begin{bmatrix} b_{p+1;ai}^+ \\ b_{m+1;ai}^- \\ b_{m+2;ai}^- \\ b_{p+2;ai}^+ \end{bmatrix} = \mathcal{P} \begin{bmatrix} A & B & -C & -D \\ B & A & -D & -C \\ C & D & A & B \\ D & C & B & A \end{bmatrix} \begin{bmatrix} R_{n;ai}^+ \\ R_{n;ai}^- \\ \bar{R}_{n;ai}^- \\ \bar{R}_{n;ai}^+ \end{bmatrix}, \tag{23}$$

where  $\mathcal{P}$ ,  $A$ ,  $B$ ,  $C$ , and  $D$  are defined as

$$\begin{aligned}
\mathcal{P} &= \frac{-1}{(\mathbf{E}_{ai,ai}^2 - (\omega^2 - \gamma^2)\mathbf{S}_{ai,ai}^2)^2 + 4\omega^2\gamma^2\mathbf{S}_{ai,ai}^4}, \\
A &= E_{ai,ai}(E_{ai,ai}^2 - (\omega^2 - \gamma^2)S_{ai,ai}^2), \\
B &= \omega S_{ai,ai}(E_{ai,ai}^2 - (\omega^2 + \gamma^2)S_{ai,ai}^2), \\
C &= \gamma S_{ai,ai}(E_{ai,ai}^2 + (\omega^2 + \gamma^2)S_{ai,ai}^2), \\
D &= 2\omega\gamma E_{ai,ai}S_{ai,ai}^2.
\end{aligned} \tag{24}$$

We stress that Eq. (23) defines four additional trial vectors (two Hermitian and two anti-Hermitian) in iteration  $n$ . The initial vectors are obtained with  $\mathbf{R}_0^+ = \mathbf{E}_B^{[1]+}$  and the other three components of the residual set to zero, and the set of initial trial vectors hereby obtained will of course correspond to the exact solution in the case of a truly diagonal RPA matrix.

It is instructive to consider two limiting cases: For real frequencies only trial vectors of the structure  $\mathbf{X}^{++}$  and  $\mathbf{X}^{--}$  are needed, and the preconditioner reduces to

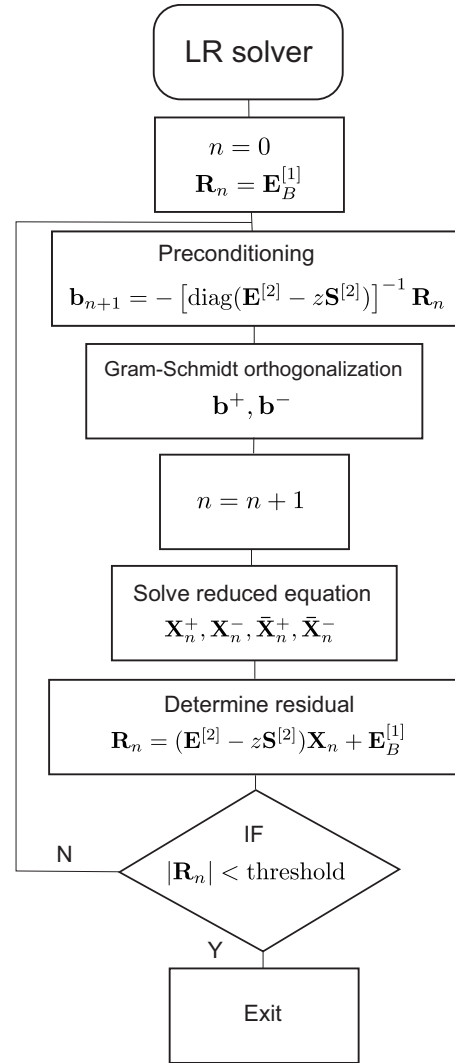


FIG. 1. Flowchart of the linear response equation solver.

$$\begin{bmatrix} b_{p+1;ai}^+ \\ b_{m+1;ai}^- \end{bmatrix} = \frac{-1}{E_{ai,ai}^2 - \omega^2 S_{ai,ai}^2} \begin{bmatrix} E_{ai,ai} & \omega S_{ai,ai} \\ \omega S_{ai,ai} & E_{ai,ai} \end{bmatrix} \begin{bmatrix} R_{n;ai}^+ \\ R_{n;ai}^- \end{bmatrix}. \tag{25}$$

For purely imaginary frequencies only components  $\mathbf{X}^{++}$  and  $\bar{\mathbf{X}}^{--}$  are needed, and the preconditioner reduces to

$$\begin{bmatrix} b_{p+1;ai}^+ \\ b_{m+1;ai}^- \end{bmatrix} = \frac{-1}{E_{ai,ai}^2 + \gamma^2 S_{ai,ai}^2} \begin{bmatrix} E_{ai,ai} & -\gamma S_{ai,ai} \\ \gamma S_{ai,ai} & E_{ai,ai} \end{bmatrix} \begin{bmatrix} R_{n;ai}^+ \\ \bar{R}_{n;ai}^- \end{bmatrix}. \tag{26}$$

## C. Details of implementation

A flowchart for the program implementation of the presented complex linear response equation solver is presented in Fig. 1. As compared to the conventional case of a real frequency,<sup>18</sup> the main difference is due to the appearance of a matrix  $i\mathbf{S}^{[2]}$  that, when multiplying a vector, will alter its time-reversal symmetry. As a consequence of this fact, a general solution vector as well as residual vector will decompose into four (and not two) components reflecting the combina-

tions of Hermiticity and time-reversal symmetry (and not only Hermiticity), and up to four trial vectors will thereby be added in each solver iteration.

Upon entering the iteration loop in the flowchart, the first program module is concerned with the preconditioning and the generation of trial vectors for the expansion of the reduced space. The generic formula for this step is given in Fig. 1, but, in order to exploit symmetries, the preconditioning matrix needs to be decomposed into matrices that alter symmetries in well-defined ways. The resulting preconditioner is given in Eq. (23).

The next module in the flowchart is concerned with orthogonalization of the trial vectors. Vectors of different Hermiticity are orthogonal by construction so the orthogonalization is carried out independently within the two groups of trial vectors (Hermitian and anti-Hermitian). By default, we choose to normalize trial vectors at this stage, and care must then be exercised if, before the normalization, the norm of a trial vector is small, since small numerical errors in the Gram–Schmidt procedure may be enlarged by the multiplication with a (large) normalization factor. We address this issue by performing a second Gram–Schmidt orthogonalization.

All the central processing unit intensive work is localized to the program module concerned with the solution of the reduced equation, more precisely the construction of the reduced Hessian matrix. For this part of the program we need to multiply the trial vector by the full-dimensional Hessian. However, there is in principle no difference encountered here compared to the conventional case of a real frequency; we are merely generating up to two Hermitian and two anti-Hermitian trial vectors in each iteration instead of one of each kind. This represents a relatively small and localized modification of the existing program code, and the technique of identifying the Hessian matrix times a trial vector by the elements of a modified Fock matrix remains intact.<sup>18</sup>

### III. COMPUTATIONAL DETAILS

The property calculations were carried out at the Hartree–Fock, DFT/CAMB3LYP,<sup>22</sup> and DFT/B3PW91 (Refs. 23 and 24) levels of theory with use of a modified version of the DIRAC program.<sup>25</sup> Hartree–Fock calculations for LiH were carried out by explicit construction of the electronic Hessian in the DIRAC program (in the nonrelativistic limit, or the Lévy–Leblond approximation) and subsequent use of a separate program implementation of the complex linear response equation solver. The dimension of the  $\mathbf{E}^{[2]}$ -matrix is in this case  $1024 \times 1024$ . Nonrelativistic and relativistic Hartree–Fock and DFT calculations of dispersion coefficients for the alkali dimers were carried out with the DIRAC program without use of external auxiliary programs. The relativistic results were obtained using the four-component Dirac–Coulomb Hamiltonian with Gaussian charge distributions representing atomic nuclei.<sup>26</sup>

Fully decontracted basis sets with exponents taken from the polarization basis set of Sadlej<sup>27,28</sup> were employed for lithium and hydrogen. For rubidium and cesium, we employed decontracted large-component basis sets with expo-

nents taken from the valence triple- $\zeta$  basis sets of Dyall.<sup>29</sup> The basis set for Rb was further augmented with one  $p$ - and two  $d$ -functions of diffuse character, and sizes of the employed basis sets equaled  $[29s22p15d2f]$  and  $[32s25p16d2f]$  for Rb and Cs, respectively. Small component basis sets were generated with use of the condition of restricted kinetic balance.

Based on the results for the electric-dipole polarizability, we determined  $C_6$  dispersion coefficients for the alkali dimers with use of the 12-point Gauss–Legendre quadrature scheme for the integration over the imaginary frequency axis. For the mapping of frequencies to the interval  $[-1,1]$ , we adopted the strategy which was proposed in Ref. 30 and used in Refs. 14 and 16.

All calculations refer to the experimental bond lengths of 1.5949,<sup>31</sup> 4.2099,<sup>32,33</sup> and 4.6462 Å (Ref. 34) for LiH, Rb<sub>2</sub>, and Cs<sub>2</sub>, respectively.

## IV. RESULTS AND DISCUSSION

### A. Lithium hydride

Lithium hydride is here used to exemplify the performance of the proposed complex linear response equation solver. We will be concerned with the situation of an perturbing electric field with frequency  $\omega$  in the electric-dipole approximation and study the induced polarization along the interatomic bond axis [denoted by  $\alpha_{zz}(\omega)$ ]. The imaginary part of the polarizability tensor is associated with the linear absorption cross section according to

$$\sigma(\omega) = \frac{4\pi\omega}{c} \text{Im}[\bar{\alpha}(\omega)], \quad (27)$$

and the parallel component of  $\alpha$  refers to absorption as due to an electric field polarized along the bond axis. In the static limit the imaginary part of  $\alpha$  vanishes in accordance with there being no absorption in a quantum mechanical system from a static electric field. In the vicinity of electronic resonances, on the other hand,  $\text{Im}[\alpha]$  will be large and show absorption peaks with Lorentzian band profiles. The half-width at half maximum equals the value of the damping parameter  $\hbar\gamma$ , which we have set equal to 0.1360 eV in the present work. The value of the damping parameter is in practical applications chosen as to reflect the resolution in the experiment and a value around 0.1 eV is commonly used to accommodate for the various broadening mechanisms in the experiment.

With the given orientation of the electric field, the lowest electronic transition in LiH with significant intensity is the  $X^1\Sigma^+ \rightarrow A^1\Sigma^+$  transition. This transition corresponds to an electronic transition from the bonding to the antibonding  $\sigma$ -orbital. In the Hartree–Fock approximation, the transition energy for this excitation is equal to about 4.0 eV, which is seen as the position of the dominant peak in the ultraviolet absorption spectrum in panel A of Fig. 2. We note that the corresponding experimental result is equal to 3.29 eV.<sup>31</sup> The discrepancy thus amounts to about 0.7 eV for this property, but, well aware of the methodological limitations, we stress that the present wave function parametrization is made mostly for pedagogical reasons. Electronic excitations to vir-

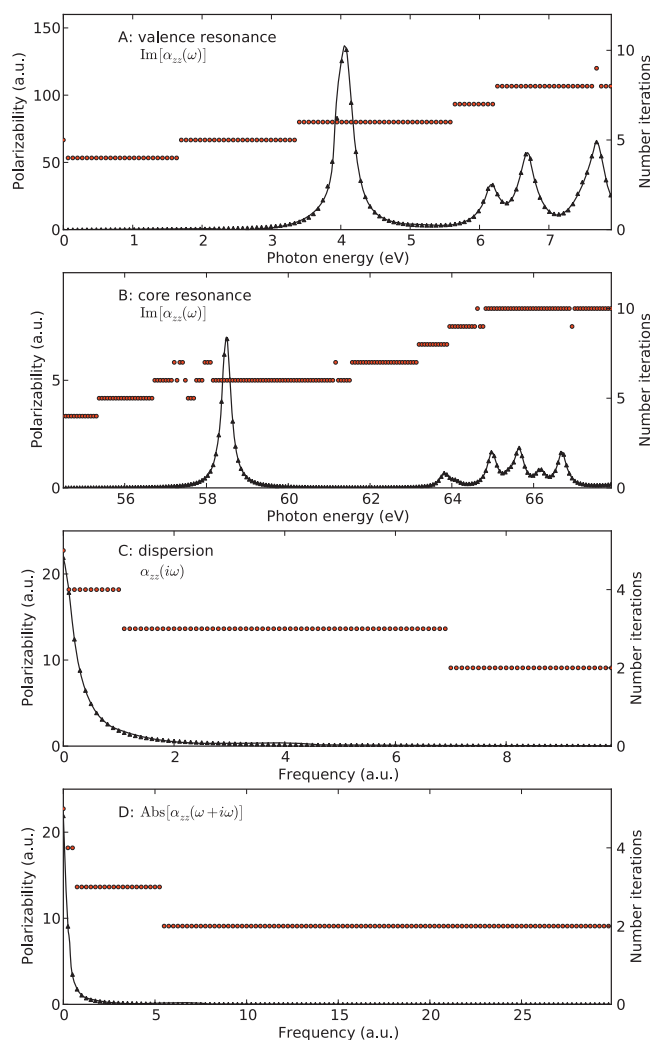


FIG. 2. Polarizability (solid line) of lithium hydride at the Hartree–Fock level of theory together with the number of iterations (circles) required in the linear response equation solver to converge to a residual norm below  $1.0 \times 10^{-3}$  a.u.

tual orbitals higher in energy give rise to the resonances seen at energies above 6.0 eV but they are all acquiring smaller intensities as compared to the lowest transition.

Also in panel A of Fig. 2, we display the number of iterations needed to converge the linear equation solver to a residual norm below  $1.0 \times 10^{-3}$  a.u. This convergence threshold is prototypical for linear response calculations and guarantees at least three digits accuracy in the resulting linear response equation. We remark that the residual in iteration  $n$  being the sum of the four components given in Eq. (21) according to

$$\mathbf{R}_n = \mathbf{R}_n^+ + \mathbf{R}_n^- + i(\bar{\mathbf{R}}_n^+ + \bar{\mathbf{R}}_n^-). \quad (28)$$

In the static limit, the solver requires five iterations to converge as indicated by the left-most solid circle in panel A (this circle lies on the y-axis in the figure). With the introduction of a finite frequency in the calculation, the number of iterations required for convergence drops to four (for frequencies corresponding to photon energies less than about 1.7 eV). This improved convergence rate is associated with the fact that diagonal approximation of the RPA matrix be-

comes more accurate with increasing contributions from the diagonal metric [see discussion below Eq. (6)]. As the frequency continues to grow closer to an electronic resonance, however, this effect is counterbalanced by the singularity of the RPA matrix for real frequency arguments equal to any of the transition energies. With inclusion of the small damping term  $i\gamma$  in the frequency argument, we pass closely by these singularities in the complex frequency plane. Upon passing the first intense  $X \ ^1\Sigma^+ \rightarrow A \ ^1\Sigma^+$  resonance, the number of iterations needed for convergence is seen to increase to six, and in the energy region between 6 and 8 eV, where the density of states is higher, the iteration count grows to eight (and in one case nine).

Panel B of Fig. 2 is used to illustrate the application of the CPP approach to address soft x-ray pre-edge absorption spectroscopies. In the present example we are concerned with  $1s$ -core resonances of lithium and the first absorption peak in the spectrum occurs at about 58.2 eV and is associated by the electronic transition  $1s \rightarrow \sigma^*$ . We note that the intensities in x-ray absorption spectra are in general small in comparison to peaks in visible/ultraviolet absorption spectra due to the reduced overlap of initial- and final-state electron densities.

The observed core-valence transition energy is in good agreement with the prominent peak at 58.4 eV in the photoelectron yield spectrum reported by Ichikawa *et al.*<sup>35</sup> for crystal LiH. But, since our results are based on the electron uncorrelated Hartree–Fock approximation, such a close agreement is fortuitous. Because, a second characteristic of core transitions (as compared to valence transitions) is that they are associated with strong electronic relaxation in the excited state, i.e., with the ground state as reference, the valence electrons will flow in the direction of the core hole in the formation of the excited state. This strong hole-electron correlation makes uncorrelated CPP calculations rather pointless, but they are carried out here to illustrate the convergence issues of the proposed solver algorithm. A relatively accurate treatment of the hole-electron correlation has been demonstrated by use of the CAMB3LYP exchange-correlation functional with parameter settings that provide a correct asymptotic limit of the Coulomb interaction.<sup>9,36</sup>

A third characteristic in concern with x-ray absorption spectroscopies is that the semibound excited states are embedded in a continuum of valence ionized states, so that the density of states is high. In view of the results in panel B, however, we note that the stability of the equation solver is not significantly affected by this fact. Below the first core-excitation resonance the solver requires four iterations to reach convergence, in the region of the first resonance this number increases to 5–7, and in the region of the high-lying bands the number of iterations becomes equal to 8–10. This convergence behavior parallels that observed for the ultraviolet region with a tendency for a need of 1–2 additional iterations in the x-ray region.

As mentioned in Sec. I, it is with the complex linear response solver also possible to address dispersion interactions. For the determination of  $C_6$  electric dipole dispersion coefficients, the needed molecular property is the polarizability evaluated on the imaginary frequency axis which merely

TABLE I. Static polarizabilities (a.u.) and  $C_6$  dispersion coefficients ( $10^3$  a.u.) for the rubidium dimer. Theoretical results refer to nonrelativistic (NR) and one-(1C) and four-component (4C) calculations.

Method		$\alpha_{\perp}$	$\alpha_{\parallel}$	$\bar{\alpha}$	$C_6$	
This work	HF	NR	576.5	921.6	691.5	20.5
		4C	548.5	895.1	664.1	19.4
	B3PW91	NR	417.3	792.2	542.2	14.4
		4C	393.8	761.3	516.3	13.5
	CAMB3LYP	NR	432.9	784.9	550.2	14.8
		4C	409.3	759.3	525.9	14.0
Jiemchoorj <sup>a</sup>	B3PW91	NR	447.7	801.5	565.6	15.3
	CCSD	NR	429.4	888.5	582.4	16.7
Deiglmayr <sup>b</sup>	CI	1C <sup>c</sup>	405.5	789.7	533.5	
Lim <sup>d</sup>	B3LYP	1C <sup>c</sup>	394.4	761.1	516.6	
		PW91	1C <sup>e</sup>	425.9	790.2	547.4
	CCSD(T) <sup>f</sup>	1C <sup>e</sup>	419.9	815.2	551.6	
Tarnovsky <sup>g</sup>	Expt <sup>h</sup>			533.1 ± 40.5 (527 K)		

<sup>a</sup>Reference 37.<sup>b</sup>Reference 42.<sup>c</sup>Using effective core potential and including mass velocity, and Darwin relativistic corrections.<sup>d</sup>Reference 41.<sup>e</sup>Using effective core potential.<sup>f</sup>A CCSD(T) result by Urban and Sadlej from 1995 is also available but considered as less reliable.<sup>g</sup>Reference 46.<sup>h</sup>An experimental result by Molof *et al.* from 1974 is also available but considered as less reliable.

constitutes a special case of application for a general complex linear response solver with  $z=i\omega$ . In the static limit, this calculation is of course identical to the regular polarizability calculation discussed above and presented in Panel A (which required 5 iteration to reach convergence). For finite frequencies, however, there is a fundamental difference in that there are no singular points of the RPA matrix to be found on the imaginary frequency axis. The dispersion of  $\alpha(i\omega)$  is not only smooth but also monotonous, see panel C for the case of LiH. As a consequence of this fact, the number of required iterations decrease first to 4 for small frequencies (in accordance with case of real frequencies presented in Panel A), but, since for larger frequencies the preconditioner in Eq. (23) will become ever more accurate, the number of required iterations will keep reducing. In a 12-point Gauss–Legendre quadrature scheme (with the adopted mapping of frequencies) the largest required frequency is about 32.23 a.u., and in panel C we note that, at such large frequency values, the solver will require no more than 2 iterations to reach convergence.

Finally, with respect to our case study of LiH, we illustrate in panel D calculations of  $\alpha(z)$  with  $z=\omega+i\omega$ . The take-home message in this example is that the favorable convergence behavior observed above for calculations of dispersion interactions is not connected with the frequency being purely imaginary but rather its separation from the singularities of the RPA matrix.

## B. Rb<sub>2</sub> and Cs<sub>2</sub>

The rubidium and cesium dimers form covalent bonds with the 5s and 6s atomic orbitals, respectively, which, in that respect, puts them on equal footing with the silver and gold dimers. The polarizabilities of these alkali dimers have been determined by several others, both theoretically and

experimentally, but, to the best of our knowledge, there exists no prior report of dispersion interaction coefficients aside from our previous nonrelativistic result for Rb<sub>2</sub>. With respect to theoretical polarizability results, we improve on earlier results by inclusion of nonscalar relativistic effects beyond the use of effective core potentials.

Our results for the static polarizabilities of Rb<sub>2</sub> and Cs<sub>2</sub> are presented in Tables I and II, respectively, together with a collection of previous theoretical and experimental values taken from the literature. We have made a previous contribution to the set of theoretical data for the rubidium dimer<sup>37</sup> where we performed nonrelativistic DFT calculations using the hybrid B3PW91 exchange–correlation functional. The choice of functional was motivated by theoretical–experimental comparisons of property results (polarizabilities and  $C_6$  coefficients) for several closed-shell alkali metal clusters.<sup>37,38</sup> For reasons of comparison as well as documented quality in the present context, we employ this functional also in the present work, but, at the same time, we extend our study by adopting the recently developed CAMB3LYP functional which by means of Coulomb attenuation provides an accurate description of electron correlation in time-dependent DFT. As a rule of thumb, when it comes to optical properties, one can expect DFT/CAMB3LYP to deliver results of comparable accuracy as the coupled cluster singles and doubles approach,<sup>39,40</sup> and, in the present work, we consider the DFT/CAMB3LYP results to be the most accurate.

Correlation effects are very strong for Rb<sub>2</sub> and Cs<sub>2</sub> causing large reductions in property values—the effect of electron correlation reduces  $\alpha_{\perp}$ ,  $\alpha_{\parallel}$ , and  $\bar{\alpha}$  by about 25%–30%, 15%, and 20%–24%, respectively. The direct comparison with other theoretical results is made difficult for several reasons: first and foremost, one can in general not separate effects of correlation from effects of relativity, but, in addi-

TABLE II. Static polarizabilities (a.u.) and  $C_6$  dispersion coefficients ( $10^3$  a.u.) for the cesium dimer. Theoretical results refer to nonrelativistic (NR) and one-(1C) and four-component (4C) calculations.

Method			$\alpha_{\perp}$	$\alpha_{\parallel}$	$\bar{\alpha}$	$C_6$
This work	HF	NR	818.5	1294.0	977.0	35.1
		4C	726.8	1205.9	886.5	30.9
	B3PW91	NR	566.0	1116.6	749.5	23.9
		4C	494.4	1006.5	665.1	20.6
	CAMB3LYP	NR	605.7	1100.6	770.6	25.2
		4C	530.9	1016.8	692.8	21.9
Deiglmayr <sup>a</sup>	CI	1C <sup>b</sup>	509.0	1012.2	676.7	
Lim <sup>c</sup>	B3LYP	1C <sup>d</sup>	505.7	1022.6	678.0	
		PW91	1C <sup>d</sup>	538.7	1040.7	706.1
	CCSD(T)	1C <sup>d</sup>	536.9	1073.7	715.8	
		Expt <sup>f</sup>				701.8 ± 54.0 (480 K)

<sup>a</sup>Reference 42.<sup>b</sup>Using effective core potential and including mass velocity, and Darwin relativistic corrections.<sup>c</sup>Reference 41.<sup>d</sup>Using effective core potential.<sup>e</sup>Reference 46.<sup>f</sup>An experimental result by Molof *et al.* from 1974 is also available but considered as less reliable.

tion, authors have adopted different internuclear separations in their respective work. Concerning the latter aspect, we note that for the rubidium dimer both Lim *et al.*<sup>41</sup> and Jiemchoorj<sup>37</sup> used a bond length separation of 4.18 Å whereas we and also Deiglmayr<sup>42</sup> have adopted a value of 4.2099 Å, as taken from a relatively recent experiment.<sup>32,33</sup> With regard to relativistic effects, our work stands out for its consideration of nonscalar, that is, spin-orbit effects.

The combined spin-orbit and molecular field splittings in the  $4p$ -shell of  $Rb_2$  reach values up to about 1.0 eV as indicated by the orbital energies at the four-component DFT/CAMB3LYP level of theory. The effect due to the molecular field, however, is small in comparison to that of spin-orbit interactions. An estimate of the molecular field splittings is obtained by considering the nonrelativistic orbital energies which point at a value of about 0.15 eV. We also find the same value from a scalar relativistic calculations, so there are clearly large changes in the energetics of the valence shells due to spin-orbit interactions, and which in turn affect results for valence molecular properties of the rubidium dimer. The best theoretical results for the isotropic average of the polarizability of  $Rb_2$  fall in between our four-component DFT/CAMB3LYP value of 525.9 a.u. and the one-component CCSD(T) result of 551.6 a.u., see Table I. The best experimental result available for the same property is 533.1 a.u. This experimental result is obtained at a temperature of 527 K, and, if extrapolated to 0 K, it is expected to become somewhat reduced.

For the cesium dimer the orbital energy splittings in the  $5p$ -shell are within 1.8 eV at the DFT/CAMB3LYP level of theory. As discussed above, this splitting is predominantly due to spin-orbit interactions but there is also a small effect due to the molecular fields—the latter effect is in this case estimated to be about 0.18 eV. In view of these values, it appears critical to include nonscalar relativistic effects in the determination of valence optical properties of the cesium dimer. The best theoretical results for  $\bar{\alpha}$  of  $Cs_2$  in the static limit are the one-component configuration interaction value

of 676.7 a.u. and the one-component CCSD(T) value of 715.8 a.u. together with our four-component DFT/CAMB3LYP value of 692.8 a.u. The best experimental result for this property is recorded at a temperature of 480 K and amounts to 701.8 a.u. Just as for the rubidium dimer, the experiment is performed on an ensemble of rovibrationally excited molecules and one can anticipate a reduced result in the limit of zero temperature.

To the best of our ability, we conclude that our four-component DFT/CAMB3LYP results for the polarizabilities of the alkali metal dimers represent the current state-of-the-art in terms of accuracy. Based on the isotropic averages of the polarizability, we determine the long-range dipole dispersion interaction coefficient from the leading term in the Casimir–Polder integral<sup>43</sup>

$$C_6 = \frac{3\hbar}{\pi} \int_0^{\infty} \bar{\alpha}^2(i\omega) d\omega, \quad (29)$$

and our best results for  $C_6$  amounts to  $14.0 \times 10^3$  and  $21.9 \times 10^3$  a.u. for  $Rb_2$  and  $Cs_2$ , respectively. In the London approximation, the  $C_6$  coefficient relates to the polarizability according to the simple expression

$$C_6 = \frac{3\omega_1}{4} \bar{\alpha}^2(0), \quad (30)$$

where  $\omega_1$  is an effective frequency that sometimes is associated with electron ionization energies.<sup>44</sup> It has been shown that this frequency can be regarded as a quite universal parameter for an entire class of systems as in the cases of  $n$ -alkanes<sup>16,45</sup> and sodium clusters.<sup>38</sup> Given the results presented in Tables I and II our DFT/CAMB3LYP estimates for  $\omega_1$  become equal to 0.0675 and 0.0608 a.u. for  $Rb_2$  and  $Cs_2$ , respectively.

## V. CONCLUSIONS

We have presented an algorithm for the solution of the linear response equation in the random phase approximation

that avoids direct matrix inversion by use of matrix-vector multiplications in an iterative scheme. The algorithm is general in the sense that it allows for arbitrary complex frequency arguments as well as matrix and vector elements, and, in the present work, it has been employed in the context of four-component, noncollinear, density functional theory. Time-reversal symmetry in the wave function and Hermiticity in operators are exploited in ways that the reduced space equation becomes real-valued. The algorithm is, by numerical examples, shown to be robust and efficient in applications regarding visible, ultraviolet, and x-ray spectroscopies as well as for the determination of dispersion interaction coefficients.

We provide theoretical estimates for the polarizability of the rubidium and cesium dimers in the limit of static frequencies and zero temperature. Our best results for this isotropic average of the property, and obtained at the four-component DFT/CAMB3LYP level of theory, read as 525.9 and 692.8 a.u. for Rb<sub>2</sub> and Cs<sub>2</sub>, respectively. These results are in perfect agreement with the most recent experimental estimates. By direct determination of the polarizability tensor for imaginary frequency arguments, the corresponding C<sub>6</sub> dispersion interaction coefficients are estimated to equal  $14.0 \times 10^3$  and  $21.9 \times 10^3$  a.u. for Rb<sub>2</sub> and Cs<sub>2</sub>, respectively.

## ACKNOWLEDGMENTS

P.N. acknowledges financial support from the Swedish Research Council (Grant No. 621-2007-5269), S.V. acknowledges a postdoctoral scholarship from the Carl Trygger Foundation (Grant No. CTS 09:274), and T.S. acknowledges the work as part of the WADEMECOM project that is funded by the Agence Nationale de la Recherche (ANR), France. The authors acknowledge a grant for computing time from National Supercomputer Centre (NSC), Sweden.

- <sup>1</sup>P. Norman, D. M. Bishop, H. J. Aa. Jensen, and J. Oddershede, *J. Chem. Phys.* **123**, 194103 (2005).
- <sup>2</sup>P. Norman, D. M. Bishop, H. J. Aa. Jensen, and J. Oddershede, *J. Chem. Phys.* **115**, 10323 (2001).
- <sup>3</sup>J. Autschbach, L. Jensen, G. C. Schatz, Y. C. E. Tse, and M. Krykunov, *J. Phys. Chem. A* **110**, 2461 (2006).
- <sup>4</sup>A. Devarajan, A. Gaenko, and J. Autschbach, *J. Chem. Phys.* **130**, 194102 (2009).
- <sup>5</sup>K. Kristensen, J. Kauczor, T. Kjærgaard, and P. Jørgensen, *J. Chem. Phys.* **131**, 044112 (2009).
- <sup>6</sup>L. Jensen, L. L. Zhao, J. Autschbach, and G. C. Schatz, *J. Chem. Phys.* **123**, 174110 (2005).
- <sup>7</sup>A. Mohammed, H. Ågren, and P. Norman, *Chem. Phys. Lett.* **468**, 119 (2009).
- <sup>8</sup>U. Ekström, P. Norman, V. Carravetta, and H. Ågren, *Phys. Rev. Lett.* **97**, 143001 (2006).
- <sup>9</sup>U. Ekström and P. Norman, *Phys. Rev. A* **74**, 042722 (2006).
- <sup>10</sup>A. Jiemchoorj, U. Ekström, and P. Norman, *J. Chem. Phys.* **127**, 165104 (2007).

- <sup>11</sup>A. Jiemchoorj and P. Norman, *J. Chem. Phys.* **128**, 234304 (2008).
- <sup>12</sup>P. Norman, K. Ruud, and T. Helgaker, *J. Chem. Phys.* **120**, 5027 (2004).
- <sup>13</sup>M. Krykunov, M. D. Kundrat, and J. Autschbach, *J. Chem. Phys.* **125**, 194110 (2006).
- <sup>14</sup>A. Jiemchoorj and P. Norman, *J. Chem. Phys.* **126**, 134102 (2007).
- <sup>15</sup>S. Villaume and P. Norman, *Chirality* **21**, E13 (2009).
- <sup>16</sup>P. Norman, A. Jiemchoorj, and B. E. Sernelius, *J. Chem. Phys.* **118**, 9167 (2003).
- <sup>17</sup>P. Jørgensen, H. J. Aa. Jensen, and J. Olsen, *J. Chem. Phys.* **89**, 3654 (1988).
- <sup>18</sup>T. Saue and H. J. Aa. Jensen, *J. Chem. Phys.* **118**, 522 (2003).
- <sup>19</sup>T. Saue, in *Relativistic Electronic Structure Theory-Part 1: Fundamentals*, edited by P. Schwerdtfeger (Elsevier, Amsterdam, 2002), Chap. 7.
- <sup>20</sup>R. Bast, H. J. Aa. Jensen, and T. Saue, *Int. J. Quantum Chem.* **109**, 2091 (2009).
- <sup>21</sup>T. Saue and H. J. Aa. Jensen, *J. Chem. Phys.* **111**, 6211 (1999).
- <sup>22</sup>T. Yanai, D. P. Tew, and N. C. Handy, *Chem. Phys. Lett.* **393**, 51 (2004).
- <sup>23</sup>A. D. Becke, *J. Chem. Phys.* **98**, 5648 (1993).
- <sup>24</sup>J. P. Perdew, J. A. Chevary, S. H. Vosko, K. A. Jackson, M. R. Pederson, and D. J. Singh, *Phys. Rev. B* **46**, 6671 (1992).
- <sup>25</sup>See <http://dirac.chem.sdu.dk> for DIRAC, a relativistic *ab initio* electronic structure program, release DIRAC08 (2008), written by L. Visscher, H. J. Aa. Jensen, and T. Saue, with new contributions from R. Bast, S. Dutilleul, K. G. Dyall, U. Ekström, E. Eliav, T. Fleig, A. S. P. Gomes, T. U. Helgaker, J. Henriksson, M. Iliaš, Ch. R. Jacob, S. Knecht, P. Norman, J. Olsen, M. Pernpointner, K. Ruud, P. Salek, and J. Sikkema.
- <sup>26</sup>L. Visscher and K. G. Dyall, *At. Data Nucl. Data Tables* **67**, 207 (1997).
- <sup>27</sup>A. J. Sadlej, *Collect. Czech. Chem. Commun.* **53**, 1995 (1988).
- <sup>28</sup>A. J. Sadlej and M. Urban, *J. Mol. Struct.: THEOCHEM* **234**, 147 (1991).
- <sup>29</sup>K. G. Dyall, *J. Phys. Chem. A* **113**, 12638 (2009).
- <sup>30</sup>R. D. Amos, N. C. Handy, P. J. Knowles, J. E. Rice, and A. J. Stone, *J. Phys. Chem.* **89**, 2186 (1985).
- <sup>31</sup>K. P. Huber and G. Herzberg, *Molecular Spectra and Molecular Structure: IV. Constants of Diatomic Molecules* (Van Nostrand, New York, 1979).
- <sup>32</sup>J. Y. Seto, R. J. Le Roy, J. Vergès, and C. Amiot, *J. Chem. Phys.* **113**, 3067 (2000).
- <sup>33</sup>C. Amiot, P. Crozet, and J. Vergès, *Chem. Phys. Lett.* **121**, 390 (1985).
- <sup>34</sup>C. Amiot and O. Dulieu, *J. Chem. Phys.* **117**, 5155 (2002).
- <sup>35</sup>K. Ichikawa, N. Suzuki, and K. Tsutsumi, *J. Phys. Soc. Jpn.* **50**, 3650 (1981).
- <sup>36</sup>G. Tu, Z. Rinkevicius, O. Vahtras, H. Ågren, U. Ekström, P. Norman, and V. Carravetta, *Phys. Rev. A* **76**, 022506 (2007).
- <sup>37</sup>A. Jiemchoorj, B. E. Sernelius, and P. Norman, *J. Comput. Methods Sci. Eng.* **7**, 475 (2007).
- <sup>38</sup>A. Jiemchoorj, P. Norman, and B. E. Sernelius, *J. Chem. Phys.* **125**, 124306 (2006).
- <sup>39</sup>M. J. Paterson, O. Christiansen, F. Pawłowski, P. Jørgensen, C. Hättig, T. Helgaker, and P. Salek, *J. Chem. Phys.* **124**, 054322 (2006).
- <sup>40</sup>J. Henriksson, T. Saue, and P. Norman, *J. Chem. Phys.* **128**, 024105 (2008).
- <sup>41</sup>I. S. Lim, P. Schwerdtfeger, T. Shnel, and H. Stoll, *J. Chem. Phys.* **122**, 134307 (2005).
- <sup>42</sup>J. Deiglmayr, M. Aymar, R. Wester, M. Weidemüller, and O. Dulieu, *J. Chem. Phys.* **129**, 064309 (2008).
- <sup>43</sup>H. B. G. Casimir and D. Polder, *Phys. Rev.* **73**, 360 (1948).
- <sup>44</sup>G. Mahan and K. Subbaswamy, *Local Density Theory of Polarizability* (Plenum, New York, 1990).
- <sup>45</sup>A. Jiemchoorj, B. E. Sernelius, and P. Norman, *Phys. Rev. A* **69**, 044701 (2004).
- <sup>46</sup>V. Tarnovsky, M. Bunimovicz, L. Vušković, B. Strumpf, and B. Bederson, *J. Chem. Phys.* **98**, 3894 (1993).